Published in final edited form as:
Kidney Int. 2013 January ; 83(1): 72–83. doi:10.1038/ki.2012.328.

In vivo multiphoton imaging of mitochondrial structure and function during acute kidney injury

Andrew M. Hall[1], **George J. Rhodes**[2], **Ruben M. Sandoval**[2], **Peter R. Corridon**[2], and **Bruce A. Molitoris**[2]

[1]University College London Centre for Nephrology, Royal Free Hospital, London, UK

[2]Division of Nephrology, Department of Medicine, Indiana Center for Biological Microscopy, Indiana University School of Medicine, Indianapolis, Indiana, USA

Abstract

Mitochondrial dysfunction has been implicated in the pathogenesis of acute kidney injury due to ischemia and toxic drugs. Methods for imaging mitochondrial function in cells using confocal microscopy are well established; more recently, it was shown that these techniques can be utilized in *ex vivo* kidney tissue using multiphoton microscopy. We extended this approach *in vivo* and found that kidney mitochondrial structure and function can be imaged in anesthetized rodents using multiphoton excitation of endogenous and exogenous fluorophores. Mitochondrial nicotinamide adenine dinucleotide increased markedly in rat kidneys in response to ischemia. Following intravenous injection, the mitochondrial membrane potential–dependent dye TMRM was taken up by proximal tubules; in response to ischemia, the membrane potential dissipated rapidly and mitochondria became shortened and fragmented in proximal tubules. In contrast, the mitochondrial membrane potential and structure were better maintained in distal tubules. Changes in mitochondrial structure, nicotinamide adenine dinucleotide, and membrane potential were found in the proximal, but not distal, tubules after gentamicin exposure. These changes were sporadic, highly variable among animals, and were preceded by changes in non-mitochondrial structures. Thus, real-time changes in mitochondrial structure and function can be imaged in rodent kidneys *in vivo* using multiphoton excitation of endogenous and exogenous fluorophores in response to ischemia–reperfusion injury or drug toxicity.

Keywords

acute kidney injury; gentamicin; *in vivo* microscopy; ischemia; mitochondria; multiphoton imaging

Correspondence: Andrew M. Hall, University College London Centre for Nephrology, Royal Free Hospital, Rowland Hill Street, London NW3 2PF, UK. andrew.hall@ucl.ac.uk.

DISCLOSURE

All the authors declared no competing interests.

SUPPLEMENTARY MATERIAL

Movie S1. Cell shedding in the rat PT following ischemia-reperfusion injury.

Supplementary material is linked to the online version of the paper at http://www.nature.com/ki

Mitochondria have a variety of important intracellular functions, including ATP production (via oxidative phosphorylation), synthesis of reactive oxygen species (ROS), modulation of Ca^{2+} signals, and regulation of cell death pathways (for review see Duchen *et al.*[1]). Mitochondrial dysfunction has been implicated in the pathogenesis of a range of renal diseases, including ischemic-[2–7] and drug-induced[8,9] acute kidney injury (AKI). The proximal tubule (PT) is densely packed with mitochondria and is frequently the major site of damage in AKI. To understand more about the underlying mechanisms and develop novel protective strategies, new technological approaches are required that will enable the study of mitochondrial function in the kidney *in vivo* in animal models of AKI.

Previous studies on mitochondria in the kidney have relied mainly on morphological analysis with electron microscopy, on measures of tissue oxygen consumption, or on respiratory chain function tests conducted on isolated organelles (which can become damaged during the isolation process).[10] Methods for studying a variety of mitochondrial functions *in situ* in intact cells using fluorescence microscopy are well established;[11] however, PT-derived immortalized cell lines can differ greatly in their metabolism from native PT,[12] and the usage of primary tissue is therefore preferable. Confocal microscopy of freshly isolated PTs has been used to gain important insights into the effects of hypoxia on mitochondrial function.[6,13] Multiphoton microscopy allows greater tissue penetration, with less phototoxicity, compared with conventional confocal imaging; it thus provides the potential to transfer imaging approaches established in isolated cells and tubules to intact sections of tissue. It has been demonstrated recently that a range of aspects of mitochondrial function can be imaged *ex vivo* in live slices of rat kidney[14] and intact isolated perfused organs[15] using multiphoton microscopy. Imaging intact tissue with a preserved architecture enables the direct comparison of signals between different cell types, and an initial study using this novel approach has suggested that mitochondrial function varies along the nephron, both at rest and in response to ischemia.

Multiphoton microscopy of the rodent kidney *in vivo* is now an established and powerful technique in renal research (e.g. see Molitoris *et al.*[16] and Sipos *et al.*[17]), and in the present study we have demonstrated that it can be applied to image mitochondrial function in the kidneys of anesthetized rodents, both at rest and in models of ischemia- and gentamicin-induced AKI, by using appropriate endogenous and exogenous fluorophores.

RESULTS

In vivo imaging of mitochondrial nicotinamide adenine dinucleotide (NADH) and membrane potential

The PT in the rodent kidney emits a large amount of autofluorescence *in vivo*; we found that the blue autofluorescence signal in mice and rats was dominated by mitochondrial NADH (Figure 1a and b), which was optimally excited at 720–760 nm. NADH is the substrate for respiratory chain complex I, but the oxidized form of the molecule (NAD^+) is not fluorescent;[18] hence, the emitted fluorescence signal reflects the proportion of the total NAD pool that is in a reduced state at any given time. The origin of the NADH signal was confirmed by colocalization with tetramethyl rhodamine methyl ester (TMRM) and also by a marked increase in intensity in response to ischemia (see below—‘Real-time *in vivo*

imaging of mitochondrial structure and function during ischemia-reperfusion'). Nicotinamide adenine dinucleotide phosphate (NADPH) has similar spectral properties to NADH; however, we observed relatively little blue autofluorescence signal outside the mitochondria (Figure 1b), suggesting that cytosolic NADPH does not contribute significantly to the emitted signal.

The autofluorescence signal in the green range was bright across a range of excitation wavelengths (700–850 nm) and consisted principally of two components: one mitochondrial in origin and the other non-mitochondrial, probably originating from lysosomes.[19,20] The latter signal was present only in PTs and not in the distal tubules (DTs). The mitochondrial green signal at lower excitation wavelengths (<800 nm) partly consisted of bleed-through from NADH, as the intensity was observed to increase in response to ischemia; however, there was also another component visible at higher excitation wavelengths (>800 nm) that may represent oxidized flavoproteins (FAD^{2+}),[14,21,22] but the signal was too weak to consistently define confirmatory changes in response to ischemia.

Mitochondrial membrane potential ($\Delta\psi_m$) lies at the heart of the mitochondrial function, determining the rates of key processes such as ATP production, ROS generation, and Ca^{2+} uptake. TMRM and rhodamine 123 are lipophilic cationic dyes that accumulate in the mitochondria according to $\Delta\psi_m$;[11] following intravenous injections, rapid uptake of these dyes was observed within seconds in PT cells in both mice and rats, predominantly from the basolateral side (Figure 1c – e). TMRM also loaded well into DTs and glomeruli (Figure 1c), but there was relatively little rhodamine 123 uptake into these structures (Figure 1d), suggesting that TMRM is a more useful dye for measuring $\Delta\psi_m$ in rodent kidneys *in vivo*.

Both TMRM and rhodamine 123 fluorescence signals decreased gradually over time in PTs following intravenous injection (Figure 1f). We postulated that the decay in signal in PTs could have been because of dye extrusion by cell membrane efflux pumps; TMRM and rhodamine 123 are both substrates for the MDR (P-glycoprotein),[23] and the renal tubule also contains organic cation transporters that have been shown to facilitate efflux of fluorescent cationic molecules *in vivo*.[24] However, we found that neither verapamil (an inhibitor of the MDR[25]) nor cimetidine (an inhibitor of organic cation transporters[26]) prevented the decay of TMRM signal in the PT when injected intravenously 10 min before the injection of dye; in contrast to PTs, TMRM signal in DTs did not decay over time (Figure 1g).

ROS and glutathione

The mitochondrial respiratory chain is a major source of intracellular ROS production *in vitro*,[27] but very little is known about the relative contributions of various ROS-generating pathways *in vivo*. Dihydroethidium (HEt) emits a fluorescence signal in the red range in the presence of superoxide and is widely used as a marker of intracellular ROS production. Following intravenous injection of HEt in rats, an increase in fluorescence signal was noted within minutes in tubular cells, which localized predominantly to the mitochondria (as demonstrated by colocalization with NADH), and, although the intensity of signal was heterogeneous across the cortex, it was markedly higher in PTs in comparison with adjacent DTs (Figure 2a–c). These findings are consistent (i) with mitochondria being a major source of ROS production in tubular cells *in vivo* and (ii) with a higher rate of ROS generation in

PTs than in DTs. This is in agreement with previous *ex vivo* studies on ROS production in the rodent kidney; however, *in vivo* we did not observe the nuclear HEt signal that also occurs *in vitro*.[14]

Glutathione is a major intracellular antioxidant that also has important roles in drug metabolism in the PT. Monochlorobimane (MCB) is a nonfluorescent dye that binds to glutathione to form a fluorescent adduct, and it has been used previously *in vitro* to obtain steady-state measurements of glutathione levels in tubular cells.[14] Following intravenous injection of MCB in rats, we observed an increase in fluorescence in PT cells within minutes that originated at the basolateral side and spread apically over time (Figure 2d–e), likely representing uptake of MCB bound to circulating glutathione, and/or uptake of unbound MCB that subsequently reacted with intracellular glutathione. Relatively little increase in fluorescence signal was noted in DTs. Shortly thereafter, the fluorescence signal decreased again in PT cells but increased in the tubular lumens (Figure 2f), consistent with active apical excretion of MCB/glutathione; the increase in luminal fluorescence was unlikely to represent filtered circulating MCB/glutathione as we did not observe any fluorescence signal in the vascular lumens. At 20 min after injection, the MCB signal had mostly disappeared from PTs, but the fluorescence signal remained high in endothelial cells (Figure 2g) and the dye became concentrated in the DT lumens (Figure 2h).

Real-time *in vivo* imaging of mitochondrial structure and function during ischemia reperfusion

Ischemia–reperfusion injury is a major cause of AKI in nephrology and transplantation. We explored the feasibility of imaging changes in the mitochondrial structure and function in real time in the rat kidney during ischemia– reperfusion. A ligature was placed around the left renal artery, which could be tightened to induce ischemia and then relaxed to allow reperfusion, while simultaneously acquiring images. The mitochondrial NADH signal increased rapidly and markedly in response to ischemia (Figure 3a–d), and decreased again on reperfusion. These changes confirmed the identity of the signal, and the magnitude of the signal increase observed in response to ischemia supports previous *in vitro* data showing that under resting conditions the mitochondrial NADH pool is in a relatively oxidized state in the PT.[14]

Induction of ischemia caused an abrupt decrease in the TMRM signal in PTs (Figure 3e and f), implying rapid depolarization of mitochondria in this nephron segment. The rate of signal decline was considerably faster than that observed in control experiments (Figure 1f). Very little further decrease in signal was observed over time during ischemia (Figure 3g), consistent with the previous data from kidney slices, which demonstrated that mitochondria in the PT are almost fully depolarized after only a short period of ischemia.[14] In contrast to the PT, $\Delta\psi_m$ was better maintained in the DT during ischemia in tissue slices; following the induction of ischemia, *in vivo* $\Delta\psi_m$ in DTs decreased more rapidly than in the *in vitro* studies but was still maintained for a longer duration than in PTs (Figure 3h). After 30 min of ischemia, the mitochondria in DTs *in vivo* appeared fully depolarized; however, $\Delta\psi_m$ was maintained to a greater extent in the cortical collecting ducts, as demonstrated by a

significantly higher mean mitochondrial TMRM signal intensity (24.5±5.9 A.U. vs. 9.5±5.0 A.U., $n = 3$, $P<0.05$) (Figure 3i and j).

Mitochondrial function is inextricably linked with morphology; changes in mitochondrial morphology in PTs have been described in response to hypoxia using electron microscopy[6] and in response to ischemia–reperfusion injury using confocal imaging of live kidney slices.[2] It is believed that mitochondrial fragmentation in the PT may have an important role in the release of proapoptotic factors and initiation of cell death during ischemic AKI.[3] As described above, NADH signal increased markedly in the PT in response to cessation of blood flow and we were able to utilize this bright signal to achieve sufficient optical resolution to obtain detailed images of mitochondrial morphology during ischemia. Mitochondria in the PT are normally elongated (Figure 3k) but became shortened and fragmented after just 10 min of ischemia (Figure 3l). Interestingly, although mitochondria in the DT were depolarized after 30 min of ischemia, mitochondrial morphology was comparatively well preserved compared with that in the PT (Figure 3m).

After 45 min of ischemia, kidneys preloaded with TMRM were reperfused; shortly thereafter, the mitochondrial fluorescence signal in the tubular cells was observed to increase with a parallel decrease in the cytosolic signal, implying redistribution of TMRM from the latter compartment to the former because of recommencement of respiratory chain activity and reenergization of mitochondria (Figure 3o). Cell shedding has been described in the PT during ischemia–reperfusion injury,[28] and we observed cells moving along the lumen during reperfusion. Some of these cells emitted a bright TMRM signal (Supplementary Movie S1 online), suggesting that mitochondria were energized in spite of cell detachment, consistent with the notion that these cells can remain viable.[29] Following exposure to 45 min of ischemia and 20 min of reperfusion, mitochondria in the PT remained shortened and fragmented when compared with control animals (Figure 3n).

In vivo imaging of mitochondrial structure and function in gentamicin toxicity

The kidney is a major excretory pathway for xenobiotics, and drug toxicity is an important cause of renal disease. The aminoglycoside antibiotic gentamicin is commonly associated with cases of AKI; previous *in vivo* imaging studies have demonstrated its uptake in the PT,[30] and histological and *in vitro* studies have implicated mitochondrial dysfunction as a key step in the pathogenesis of gentamicin-induced nephrotoxicity.[31–35] Furthermore, mitochondrial dysfunction is believed to occur before the onset of functional or morphological evidence of severe kidney injury.[32] We explored the effects of gentamicin on mitochondrial function in the rat kidney *in vivo* by using a well-established model (intraperitoneal injection of gentamicin 100 mg/kg once daily), which reliably produces AKI and a progressive increase in serum creatinine.[36] Animals were imaged at different time points to explore temporal changes in mitochondrial structure and function.

A marked increase in size in non-mitochondrial organelles emitting bright green autofluorescence was observed in PTs after just 1 day of gentamicin exposure (Figure 4a); these structures most likely represented enlarged lysosomes containing lipofuscin.[19,20,31] After 2 days, subtle abnormalities occurred in the luminal brush border of PTs, with more severe loss of structure in some areas; these changes became pronounced and widespread by

4 days (Figure 4a). In contrast to these abnormalities, mitochondrial structure and function were preserved after 2 days of gentamicin exposure (Figure 4a). After 4 days of exposure, there was evidence of mitochondrial dysfunction in some PTs, with abnormal structure and increased NADH signal (Figure 4a). However, these changes were sporadic and were not present in all animals at 4 days; overall, mitochondria in the majority of PTs remained well energized, and there was no significant difference in mean PT mitochondrial NADH fluorescence (day 0: 28.6±1.8 A.U.; 1–2 days: 30.6±2.0; 4 days: 29.6±4.4; $n = 4$ in all groups; $P = 0.90$) (Figure 4d) or mean mitochondrial TMRM fluorescence (day 0: 29.6±3.6 A.U.; 1–2 days: 34.0±4.0; 4 days: 21.2±3.9; $n = 4$ in all groups; $P = 0.11$) (Figure 4e).

After 6 days of gentamicin exposure, abnormalities in PT mitochondrial structure and function were observed in all rats, but the extent of these remained highly variable among animals. Furthermore, PTs containing grossly dysmorphic mitochondria with high NADH signal and low $\Delta\psi_m$ were observed to coexist directly adjacent to other PTs with normal appearances (Figure 4a), emphasizing the sporadic nature of gentamicin-induced damage in the kidney. After 8 days of gentamicin exposure, extensive cell death was observed in PTs, leading to the existence of ‘ghost tubules’ containing no viable cells (Figure 4b). Within the few surviving PTs, mitochondria were swollen and dysmorphic, and $\Delta\psi_m$ was highly variable among adjacent cells within the same tubule (Figure 4a). In contrast, mitochondrial morphology and function remained preserved within DTs and collecting ducts (Figure 4c).

In summary, these observations support the notion that gentamicin toxicity in the kidney is specifically targeted toward the PT and causes abnormalities in mitochondrial structure and function in this nephron segment; however, the timing and extent of damage is highly variable both among and within animals, and changes in other aspects of cell ultrastructure (including the apical brush border and lysosomes) precede abnormalities in mitochondria. Ultimately, these changes lead to cell death in the majority of PTs.

DISCUSSION

We have demonstrated that mitochondrial structure and function can be imaged in both mouse and rat kidneys *in vivo* using multiphoton excitation of endogenous and exogenous fluorophores. Furthermore, changes in signal can be followed in real time in response to ischemia–reperfusion injury or drug toxicity, the most common causes of AKI in nephrology and transplantation. We therefore believe that this approach will be useful in understanding the roles of mitochondria in renal diseases and in evaluating the effects of future mitochondrial targeted therapies.

Multiphoton microscopy has been used to image various aspects of kidney function in live animals;[16,17] we have now shown that it can be utilized to transfer established *in vitro* techniques for measuring mitochondrial function using fluorescence microscopy to the *in vivo* situation. Mitochondrial NADH can be imaged in the kidney and provides a readout of the redox state; optimal excitation occurred at 720–760 nm, which is in agreement with studies using other tissues.[22,37,38] The identity of the signal was confirmed by its mitochondrial localization and by characteristic changes in intensity in response to ischemia.[39] The magnitude of the increase in NADH signal supports the notion that

mitochondria in the kidney are in a relatively oxidized state under resting conditions,[14,40,41] a scenario that might help to limit the rate of ROS production by complex I of the respiratory chain.[27] Cytosolic NADPH has similar spectral properties to mitochondrial NADH;[42] however, the majority of the blue autofluorescence signal emitted by renal tubules originated from mitochondria, as described in other aerobic tissues such as the heart[22,37,43] and skeletal muscle.[38]

FAD^{2+} is another endogenous mitochondrial fluorophore that has been imaged using multiphoton microscopy in tissues such as the heart[22] and also provides information about the mitochondrial redox state. It is optimally excited at longer wavelengths such as 900 nm, as the green autofluorescence signal is dominated by NADH at shorter wavelengths.[22] Although we clearly identified a green autofluorescence signal of mitochondrial origin in renal tubules, we were unable to resolve characteristic changes in intensity expected in FAD^{2+} signal because of respiratory chain inhibition during ischemia;[14] this may be because of factors such as the relatively weak intrinsic fluorescence of FAD^{2+}, masking of the signal by other sources of green autofluorescence, and the fact that the green band-pass filter used in this study (495–540 nm) may not be optimal for detecting the emission spectra of FAD^{2+}, which has a peak at ~550nm.[44]

We found that following intravenous injection of mitochondrial dyes, such as TMRM and HEt, sufficient loading occurred in tubular cells to make useful physiological observations and measurements. Previous *in vitro* experiments in the rat kidney have suggested that the resting rate of ROS production is higher in PT cells than in DT cells and that the major sources of ROS generation are the mitochondrial respiratory chain and NADPH oxidases.[14] In accordance with this, we observed a higher fluorescence signal in the PT following injection with the superoxide-sensitive dye HEt; however, the signal localized to mitochondria only, suggesting that they form the major source of ROS generation *in vivo*, and we did not observe an increase in HEt signal in nuclei, which occurred in isolated perfused organs.[15] At present, we cannot be sure of the reason(s) for this *in vivo* versus *in vitro* difference, but possible explanations might include differences in oxygen tension, perfusion pressure, or composition of perfusate. The explanation for a higher relatively HEt signal in the PT mitochondria is also unclear at present. Mitochondrial ROS levels are determined by the rate of generation and the adequacy of antioxidant defenses; manganese superoxide dismutase is a major mitochondrially targeted antioxidant, and a previous study has demonstrated that manganese superoxide dismutase expression levels are higher in DTs than in PTs.[45,46]

Glutathione is an intracellular antioxidant with important roles in drug metabolism in the PT, and MCB has been used previously to take measurements of glutathione levels in renal tubular cells,[14] hepatocytes,[47,48] cardiac myocytes,[49,50] and neurons.[51–53] Although glutathione levels in PT cells *in vitro* are determined solely by intracellular synthesis and degradation, in vivo they are also affected by uptake of circulating glutathione, which is synthesized in the liver. The kidney removes ~90% of circulating glutathione; glomerular filtration accounts for less than a third of this; hence, PT uptake has an important role in glutathione homeostasis.[54] A previous study has suggested that uptake occurs at the basolateral PT membrane, via organic anion transporters or sodium-coupled transport, with

subsequent excretion across the apical membrane to maintain intracellular glutathione homeostasis.[55,56] In agreement with this, we found that MCB/glutathione was taken up by PT cells *in vivo* and was then rapidly transported to the tubular lumen. We were therefore unable to use MCB to make steady-state intracellular measurements of glutathione levels in the PT; however, it could potentially be utilized in future studies to investigate changes in PT glutathione metabolism and transport. In contrast to PTs, MCB fluorescence signal remained stable in endothelial cells, suggesting that it could be used to measure glutathione levels in the vasculature. Relatively little fluorescence signal was observed in DTs following MCB injection, consistent with previous studies, suggesting that glutathione levels are lower in this nephron segment than in the PT.[56] MCB can react with several intracellular low-molecular-weight thiols other than glutathione; however, experiments conducted in hepatocytes showed that only glutathione was in fact labeled by MCB.[47] Furthermore, although high-performance liquid chromatography analysis of isolated PTs loaded with MCB revealed evidence of cysteine– and mercapturate–MCB conjugates, in addition to glutathione–MCB,[55] it is more likely that the existence of these was because of subsequent metabolism of the glutathione–MCB conjugate, rather than because of direct binding of cysteine and mercapturate to MCB.[57]

To fully exploit the translational potential of imaging techniques, it is necessary to apply them to animal models of human diseases. We have demonstrated that changes in mitochondrial morphology and function can be imaged in real time in rodent models of AKI. We observed alterations in mitochondrial NADH signal and $\Delta\psi_m$ in renal tubules in response to ischemia reperfusion. During ischemia, the activity of the ATP synthase within the mitochondria reverses, and mitochondria become net consumers of ATP, hydrolyzing it to pump protons out of the inner matrix.[58,59] $\Delta\psi_m$ can therefore be maintained to an extent during ischemia in cells that can generate ATP via anaerobic metabolism; however, glycolytic enzyme activity is very low in PT cells.[60] In keeping with previous studies in both kidney slices[14] and intact perfused organs,[15] we found that $\Delta\psi_m$ dissipated rapidly in PTs *in vivo* following the onset of ischemia, with very little further change over 30 min. In contrast, $\Delta\psi_m$ was better maintained in DTs, which have greater glycolytic capacity and maintain higher levels of ATP during ischemia.[61] Interestingly, however, $\Delta\psi_m$ dissipated more quickly in DTs *in vivo* than in previous *in vitro* studies; this phenomenon might be attributable to a higher rate of ATP consumption *in vivo* (perhaps because of higher temperature—the slice work was conducted at room temperature). $\Delta\psi_m$ was maintained to a significantly greater extent in collecting ducts than in DTs after 30 min of ischemia, which could potentially be explained by a higher capacity to generate ATP anaerobically in the former nephron segment; experiments using isolated tubules have shown that the distal convoluted tubule produces relatively less lactate than the rest of the distal nephron when aerobic respiration is compromised,[62] for reasons that remain unclear.

Following an ischemic episode, cell death can subsequently occur in viable cells on reperfusion—the so-called ischemia–reperfusion injury. Mitochondria are thought to have a key role in the pathogenesis of this process,[63,64] and sustained defects in mitochondrial function have been described in the PT following hypoxia and reoxygenation.[6] We have demonstrated that changes in mitochondrial structure and function within the renal tubules

can be imaged in real time during reperfusion, and this could therefore potentially provide a powerful tool for studying the mechanisms of ischemia–reperfusion *in vivo* and for evaluating the effectiveness of potential therapeutic interventions (e.g. mitochondrially targeted antioxidants[65]). In agreement with findings from a previous study using live kidney slices, we found that mitochondria in the PT were fragmented following ischemia–reperfusion and that the TMRM signal was more heterogeneous across the cortex,[2] possibly because of variation in capillary flow resulting from microvascular damage.[66]

Drug-induced damage is a major cause of AKI, and PT mitochondria are frequently implicated as targets of toxicity.[8,9,67] We explored the effects of gentamicin, a commonly used aminoglycoside antibiotic, on mitochondrial structure and function in the kidney *in vivo*. We observed abnormalities in non-mitochondrial structures in PT cells in the first 2 days of exposure, including enlargement of lysosomes and increased autofluorescence signal in the brush border (most likely reflecting accumulation of cellular debris[31]); however, there was no significant change in mean mitochondrial NADH signal or $\Delta\psi_m$ during this time period. After 4 days, sporadic areas of altered mitochondrial morphology and increased NADH signal were observed in PTs, consistent with impaired respiratory chain activity. These abnormalities became more widespread by 6 days, and after 8 days frank necrosis occurred in PTs; in contrast, mitochondrial structure and function were preserved in DTs and collecting ducts.

Taken together, these observations are consistent with the notion that gentamicin toxicity is specifically targeted to PT and that mitochondrial dysfunction in the PT is a relatively late event in the pathogenesis of gentamicin-induced AKI but precedes the initiation of cell death. These findings are generally supported by previous studies. In PT-derived llcpk cells, gentamicin exposure caused an initial permeabilization of lysosomal membranes, which was then followed by dissipation of $\Delta\psi_m$, and subsequent activation of cell death pathways.[68] Studies using mitochondria isolated from the renal cortex have shown that abnormalities in respiratory chain function are relatively minor after 3–4 days of gentamicin exposure but become more severe after 6 days.[34,69] In addition, inhibitory effects of gentamicin on respiratory chain activity were more marked with substrates for complex I rather than for complex II;[34] impairment of complex I activity *in vivo* would push the mitochondrial NAD pool into a more reduced state, a scenario that would be consistent with the increased NADH signal that we observed in damaged PTs.

Although we found that abnormalities in mitochondrial structure and function in PTs generally occurred relatively late in the time course of gentamicin toxicity, a striking feature in our images was the high degree of variability both among and within animals exposed to the same dosage regime, as reported previously in histological studies.[31,70] Mitochondrial abnormalities in PTs occurred in some, but not all, animals after 4 days of exposure; at later time points when damage was more widespread, grossly abnormal PTs were observed to lie directly adjacent to healthy looking PTs, whereas marked variations in signal occurred among cells along the same tubule. Such a high degree of spatiotemporal heterogeneity in mitochondrial damage is unlikely to be fully appreciated by traditional means of assessing mitochondrial function in the kidney (e.g. *in vitro* respiratory chain assays using organelles isolated from kidney tissue).

There are some practical disadvantages to be considered when using an *in vivo* approach to image mitochondrial function in the kidney. Relatively large amounts of fluorescent dyes are required, and these cannot be delivered under the controlled conditions of an *in vitro* or *ex vivo* preparation. Therefore, greater heterogeneity of dye loading may be observed, and achieving a steady state within cells is more difficult; furthermore, some widely used AM ester dyes might be cleaved by extracellular enzymes *in vivo*, thus limiting their cellular uptake.[71] Rhodamine 123 is a widely used $\Delta\psi_m$-dependent dye that has been utilized previously to image mitochondria in PTs and DTs in kidney slices;[14] however, we found that this dye did not load well into DTs *in vivo* for reasons that are currently unclear. A small delayed increase in rhodamine 123 fluorescence was observed in DT cells following the appearance of filtered dye in tubular lumens, suggesting that, unlike TMRM, rhodamine 123 uptake may occur predominantly across the apical rather than basolateral membrane in these cells. This phenomenon could explain in part why rhodamine 123 uptake into DTs is greater in *in vitro* models, in which dyes are loaded by bath application rather than by vascular perfusion.

Some studies may therefore benefit initially from an *in vitro* or *ex vivo* approach under more tightly controlled conditions; however, it remains crucial that technological tools are developed and refined to allow *in vivo* confirmation of findings where possible in order to avoid inappropriate attempts to translate purely *in vitro* phenomena to the human situation. The usage of endogenous fluorophores, such as NADH, can obviously circumvent difficulties related to exogenous dye loading.

The native PT expresses an array of apical and basolateral cell membrane transporters,[72] which have the potential to extrude fluorescent dyes. Indeed, although we observed that the $\Delta\psi_m$-dependent dyes TMRM and rhodamine 123 were rapidly taken up into tubular cells and localized to the mitochondria, the fluorescence intensity subsequently decayed over time. We confirmed that this was not because of photobleaching, as the TMRM signal in DTs remained constant. The identity of PT transporter(s) responsible for extruding the dyes remains unknown at present, as inhibition of either the MDR or organic cation transporters did not prevent the signal decay.

In summary, we have demonstrated that mitochondrial structure and function can be imaged *in vivo* in rodent kidneys with multiphoton microscopy by using a combination of endogenous and exogenous fluorophores, and changes in signal can be followed in real time in established models of AKI. We have shown that this approach simultaneously facilitates quantitative analysis of global changes in mitochondrial function *in situ* across the renal cortex with detailed qualitative examination of intracellular morphology, crucially allowing the appreciation of variability in signals among different tubules and cells, which can be quite striking in diseases such as gentamicin toxicity. The potential now exists for future studies to combine measurements of mitochondrial function with other readouts in the multiphoton imaging toolkit—including blood flow, glomerular filtration rate, tubular flow, and solute transport—to build a more complete understanding of *in vivo* renal physiology and pathophysiology.

MATERIALS AND METHODS

Animals

All experiments were conducted in accordance with NIH Guidelines and were approved by the Institutional Animal Care and Use Committee. Adult male C57 mice (Harlan Labs, Indianapolis, IN) or Sprague–Dawley rats (Harlan Labs) were used (except for experiments in which Munich–Wistar rats were utilized to image superficial glomeruli). Mice weighing 20–20 g were anesthetized with inhaled isoflurane (2%), whereas rats weighing 250–400 g were anesthetized by intraperitoneal injection with thiobutabarbital sodium (Sigma Aldrich, St Louis, MO) at a dose of 160 mg/kg. They were then placed on a warming table to maintain a core temperature of 37°C, which was monitored throughout the experiment using a rectal thermometer. The right internal jugular vein was cannulated to allow the injection of fluorescent dyes.

For ischemia–reperfusion experiments, after shaving the abdomen of the rat a midline incision was made through the skin and musculature to expose the abdominal cavity. The left renal artery was isolated through blunt dissection, and a 3.0 silk suture was placed around the vessel and passed through a length of polyethylene tubing that exited the abdominal cavity. The abdomen was then closed around the tubing. To induce ischemia, the tension on the two ends of the thread was increased until there was a visible cessation of kidney perfusion; the tension was subsequently relaxed to allow reperfusion. The left kidney was externalized via a lateral incision and imaged using methods described previously.[73] For gentamicin toxicity experiments, adult male Sprague–Dawley rats weighing 250–350 g were given a daily intraperitoneal injection of gentamicin (Sigma Aldrich) at a dose of 100 mg/kg, as per a previously established protocol.[36]

Dye loading and microscope settings

Images were acquired using an inverted Fluoview 1000 Olympus microscope adapted for multiphoton microscopy (Olympus Corporation, Tokyo, Japan) and either ×20 or ×60 objectives. Fluorescent dyes were administered via intravenous injection. HEt (200 μg/ml) (Invitrogen Molecular Probes, Eugene, OR), endogenous NADH, and MCB (5 mg/ml) (Invitrogen Molecular Probes) were excited at wavelengths of 720–760nm. TMRM (5 μg/ml) and rhodamine 123 (6 μg/ml) (Invitrogen Molecular Probes) were excited at wavelengths of 800–850nm. Emitted light was collected using three fixed band-pass filters: 420–460nm (blue), 495–540nm (green), and 575–630nm (red). For experiments involving inhibitors of renal transporters, verapamil (Sigma Aldrich) was used at a dose of 1 mg/kg body weight, whereas cimetidine (Sigma Aldrich) was used at a fixed dose of 8 μmoles (0.2 ml of a 40 μM solution) per animal.

Image analysis and statistics

Images were processed using Image J software (National Institutes of Health, MD, http://rsb.info.nih.gov/ij/). Regions of interest were drawn around tubules to obtain mean fluorescence signals. Mitochondrial signals were isolated by setting a threshold level to remove the background cytosolic fluorescence. Images were acquired within 5 min of intravenous dye injection, as some signals decayed with time. To account for movement in

the z plane during ischemia experiments, images were collected in serial z-stacks and reconstructed to a signal-averaged 2D image using imaging software. For the gentamicin experiments, fields of PTs were chosen randomly using the green autofluorescence channel before obtaining NADH and TMRM signals. The results are presented as means ± s.e.m. Statistical differences among study groups were explored using oneway analysis of variance and groups were compared using the paired or unpaired *t*-test as appropriate; a P value of < 0.05 was considered significant.

Supplementary Material

Refer to Web version on PubMed Central for supplementary material.

Acknowledgments

Funding for this study was provided by an NIH P-30 O'Brien Center (DK 079312) fellowship awarded to AMH. Support for AMH was also provided by The Academy of Medical Sciences (UK).

REFERENCES

1. Duchen MR, Szabadkai G. Roles of mitochondria in human disease. Essays Biochem. 2010; 47:115–137. [PubMed: 20533904]
2. Plotnikov EY, Kazachenko AV, Vyssokikh MY, et al. The role of mitochondria in oxidative and nitrosative stress during ischemia/reperfusion in the rat kidney. Kidney Int. 2007; 72:1493–1502. [PubMed: 17914353]
3. Brooks C, Wei Q, Cho SG, et al. Regulation of mitochondrial dynamics in acute kidney injury in cell culture and rodent models. J Clin Invest. 2009; 119:1275–1285. [PubMed: 19349686]
4. Burke TJ, Wilson DR, Levi M, et al. Role of mitochondria in ischemic acute renal failure. Clin Exp Dial Apheresis. 1983; 7:49–61. [PubMed: 6883804]
5. Sun Z, Zhang X, Ito K, et al. Amelioration of oxidative mitochondrial DNA damage and deletion after renal ischemic injury by the KATP channel opener diazoxide. Am J Physiol Renal Physiol. 2008; 294:F491–F498. [PubMed: 18160622]
6. Weinberg JM, Venkatachalam MA, Roeser NF, et al. Mitochondrial dysfunction during hypoxia/reoxygenation and its correction by anaerobic metabolism of citric acid cycle intermediates. Proc Natl Acad Sci USA. 2000; 97:2826–2831. [PubMed: 10717001]
7. Devarajan P. Update on mechanisms of ischemic acute kidney injury. J Am Soc Nephrol. 2006; 17:1503–1520. [PubMed: 16707563]
8. Pfaller W, Gstraunthaler G, Willinger CC. Morphology of renal tubular damage from nephrotoxins. Toxicol Lett. 1990; 53:39–43. [PubMed: 2219185]
9. Izzedine H, Launay-Vacher V, Isnard-Bagnis C, et al. Drug-induced Fanconi's syndrome. Am J Kidney Dis. 2003; 41:292–309. [PubMed: 12552490]
10. Brand MD, Nicholls DG. Assessing mitochondrial dysfunction in cells. Biochem J. 2011; 435:297–312. [PubMed: 21726199]
11. Duchen MR, Surin A, Jacobson J. Imaging mitochondrial function in intact cells. Methods Enzymol. 2003; 361:353–389. [PubMed: 12624920]
12. Hall AM, Campanella M, Loesch A, et al. Albumin uptake in OK cells exposed to rotenone: a model for studying the effects of mitochondrial dysfunction on endocytosis in the proximal tubule? Nephron Physiol. 2010; 115:9–19.
13. Feldkamp T, Kribben A, Weinberg JM. Assessment of mitochondrial membrane potential in proximal tubules after hypoxia-reoxygenation. Am J Physiol Renal Physiol. 2005; 288:F1092–F1102. [PubMed: 15625081]

14. Hall AM, Unwin RJ, Parker N, et al. Multiphoton imaging reveals differences in mitochondrial function between nephron segments. J Am Soc Nephrol. 2009; 20:1293–1302. [PubMed: 19470684]
15. Hall AM, Crawford C, Unwin RJ, et al. Multiphoton imaging of the functioning kidney. J Am Soc Nephrol. 2011; 22:1297–1304. [PubMed: 21719788]
16. Molitoris BA, Sandoval RM. Intravital multiphoton microscopy of dynamic renal processes. Am J Physiol Renal Physiol. 2005; 288:F1084–F1089. [PubMed: 15883167]
17. Sipos A, Toma I, Kang JJ, et al. Advances in renal (patho)physiology using multiphoton microscopy. Kidney Int. 2007; 72:1188–1191. [PubMed: 17667980]
18. Chance B, Schoener B, Oshino R, et al. Oxidation-reduction ratio studies of mitochondria in freeze-trapped samples. NADH and flavoprotein fluorescence signals. J Biol Chem. 1979; 254:4764–4771. [PubMed: 220260]
19. Rice WL, Kaplan DL, Georgakoudi I. Two-photon microscopy for non-invasive, quantitative monitoring of stem cell differentiation. PLoS One. 2010; 5:e10075. [PubMed: 20419124]
20. Sandoval RM, Kennedy MD, Low PS, et al. Uptake and trafficking of fluorescent conjugates of folic acid in intact kidney determined using intravital two-photon microscopy. Am J Physiol Cell Physiol. 2004; 287:C517–C526. [PubMed: 15102609]
21. Kunz WS, Gellerich FN. Quantification of the content of fluorescent flavoproteins in mitochondria from liver, kidney cortex, skeletal muscle, and brain. Biochem Med Metab Biol. 1993; 50:103–110. [PubMed: 8373630]
22. Huang S, Heikal AA, Webb WW. Two-photon fluorescence spectroscopy and microscopy of NAD(P)H and flavoprotein. Biophys J. 2002; 82:2811–2825. [PubMed: 11964266]
23. Neyfakh AA. Use of fluorescent dyes as molecular probes for the study of multidrug resistance. Exp Cell Res. 1988; 174:168–176. [PubMed: 3335222]
24. Horbelt M, Wotzlaw C, Sutton TA, et al. Organic cation transport in the rat kidney in vivo visualized by time-resolved two-photon microscopy. Kidney Int. 2007; 72:422–429. [PubMed: 17495857]
25. Bellamy WT, Dalton WS. Multidrug resistance in the laboratory and clinic. Adv Clin Chem. 1994; 31:1–61. [PubMed: 7879670]
26. Wright SH. Role of organic cation transporters in the renal handling of therapeutic agents and xenobiotics. Toxicol Appl Pharmacol. 2005; 204:309–319. [PubMed: 15845420]
27. Murphy MP. How mitochondria produce reactive oxygen species. Biochem J. 2009; 417:1–13. [PubMed: 19061483]
28. Ashworth SL, Sandoval RM, Tanner GA, et al. Two-photon microscopy: visualization of kidney dynamics. Kidney Int. 2007; 72:416–421. [PubMed: 17538570]
29. Racusen LC. Epithelial cell shedding in acute renal injury. Clin Exp Pharmacol Physiol. 1998; 25:273–275. [PubMed: 9590582]
30. Sandoval RM, Molitoris BA. Quantifying endocytosis *in vivo* using intravital two-photon microscopy. Methods Mol Biol. 2008; 440:389–402. [PubMed: 18369960]
31. Houghton DC, Hartnett M, Campbell-Boswell M, et al. A light and electron microscopic analysis of gentamicin nephrotoxicity in rats. Am J Pathol. 1976; 82:589–612. [PubMed: 1258978]
32. Simmons CF Jr, Bogusky RT, Humes HD. Inhibitory effects of gentamicin on renal mitochondrial oxidative phosphorylation. J Pharmacol Exp Ther. 1980; 214:709–715. [PubMed: 7400973]
33. Weinberg JM, Simmons F Jr, Humes HD. Alterations of mitochondrial respiration induced by aminoglycoside antibiotics. Res Commun Chem Pathol Pharmacol. 1980; 27:521–531. [PubMed: 7384641]
34. Weinberg JM, Harding PG, Humes HD. Alterations in renal cortex cation homeostasis during mercuric chloride and gentamicin nephrotoxicity. Exp Mol Pathol. 1983; 39:43–60. [PubMed: 6223836]
35. Fujiwara K, Shin M, Matsunaga H, et al. Light-microscopic immunocytochemistry for gentamicin and its use for studying uptake of the drug in kidney. Antimicrob Agents Chemother. 2009; 53:3302–3307. [PubMed: 19451299]

36. Sandoval RM, Reilly JP, Running W, et al. A non-nephrotoxic gentamicin congener that retains antimicrobial efficacy. J Am Soc Nephrol. 2006; 17:2697–2705. [PubMed: 16971659]
37. Davidson SM, Yellon DM, Murphy MP, et al. Slow calcium waves and redox changes precede mitochondrial permeability transition pore opening in the intact heart during hypoxia and reoxygenation. Cardiovasc Res. 2012; 93:445–453. [PubMed: 22198507]
38. Piston DW, Knobel SM. Real-time analysis of glucose metabolism by microscopy. Trends Endocrinol Metab. 1999; 10:413–417. [PubMed: 10542399]
39. Franke H, Barlow CH, Chance B. Oxygen delivery in perfused rat kidney: NADH fluorescence and renal functional state. Am J Physiol. 1976; 231:1082–1089. [PubMed: 185909]
40. Coremans JM, Van AM, Naus DC, et al. Pretransplantation assessment of renal viability with NADH fluorimetry. Kidney Int. 2000; 57:671–683. [PubMed: 10652046]
41. Mayevsky A, Chance B. Oxidation-reduction states of NADH in vivo: from animals to clinical use. Mitochondrion. 2007; 7:330–339. [PubMed: 17576101]
42. Dumollard R, Ward Z, Carroll J, et al. Regulation of redox metabolism in the mouse oocyte and embryo. Development. 2007; 134:455–465. [PubMed: 17185319]
43. Eng J, Lynch RM, Balaban RS. Nicotinamide adenine dinucleotide fluorescence spectroscopy and imaging of isolated cardiac myocytes. Biophys J. 1989; 55:621–630. [PubMed: 2720061]
44. Duchen MR, Biscoe TJ. Mitochondrial function in type I cells isolated from rabbit arterial chemoreceptors. J Physiol. 1992; 450:13–31. [PubMed: 1432706]
45. Kiyama S, Yoshioka T, Burr IM, et al. Strategic locus for the activation of the superoxide dismutase gene in the nephron. Kidney Int. 1995; 47:536–546. [PubMed: 7536859]
46. Boom H, de Heer E, van der Wal A, et al. The absence of delayed graft function is predicted by the presence of manganese-superoxide dismutase in distal tubules of renal allografts. Transplantation. 2005; 79:946–952. [PubMed: 15849548]
47. Fernandez-Checa JC, Kaplowitz N. The use of monochlorobimane to determine hepatic GSH levels and synthesis. Anal Biochem. 1990; 190:212–219. [PubMed: 2291468]
48. Stevenson D, Wokosin D, Girkin J, et al. Measurement of the intracellular distribution of reduced glutathione in cultured rat hepatocytes using monochlorobimane and confocal laser scanning microscopy. Toxicol In Vitro. 2002; 16:609–619. [PubMed: 12206828]
49. Li S, Zheng MQ, Rozanski GJ. Glutathione homeostasis in ventricular myocytes from rat hearts with chronic myocardial infarction. Exp Physiol. 2009; 94:815–824. [PubMed: 19395662]
50. Sathishkumar K, Gao X, Raghavamenon AC, et al. Determination of glutathione, mitochondrial transmembrane potential, and cytotoxicity in H9c2 cardiomyoblasts exposed to reactive oxygen and nitrogen species. Methods Mol Biol. 2010; 610:51–61. [PubMed: 20013172]
51. Keelan J, Allen NJ, Antcliffe D, et al. Quantitative imaging of glutathione in hippocampal neurons and glia in culture using monochlorobimane. J Neurosci Res. 2001; 66:873–884. [PubMed: 11746414]
52. Sun X, Shih AY, Johannssen HC, et al. Two-photon imaging of glutathione levels in intact brain indicates enhanced redox buffering in developing neurons and cells at the cerebrospinal fluid and blood-brain interface. J Biol Chem. 2006; 281:17420–17431. [PubMed: 16624809]
53. Bragin DE, Zhou B, Ramamoorthy P, et al. Differential changes of glutathione levels in astrocytes and neurons in ischemic brains by two-photon imaging. J Cereb Blood Flow Metab. 2010; 30:734–738. [PubMed: 20104233]
54. Haberle D, Wahllander A, Sies H. Assessment of the kidney function in maintenance of plasma glutathione concentration and redox state in anaesthetized rats. FEBS Lett. 1979; 108:335–340. [PubMed: 520571]
55. Miller DS, Letcher S, Barnes DM. Fluorescence imaging study of organic anion transport from renal proximal tubule cell to lumen. Am J Physiol. 1996; 271:F508–F520. [PubMed: 8853412]
56. Lash LH. Role of glutathione transport processes in kidney function. Toxicol Appl Pharmacol. 2005; 204:329–342. [PubMed: 15845422]
57. Silbernagl S, Heuner A. Renal transport and metabolism of mercapturic acids and their precursors. Toxicol Lett. 1990; 53:45–51. [PubMed: 2219186]

58. Feldkamp T, Kribben A, Weinberg JM. F1FO-ATPase activity and ATP dependence of mitochondrial energization in proximal tubules after hypoxia/reoxygenation. J Am Soc Nephrol. 2005; 16:1742–1751. [PubMed: 15843467]
59. Campanella M, Parker N, Tan CH, et al. IF(1): setting the pace of the F(1)F(o)-ATP synthase. Trends Biochem Sci. 2009; 34:343–350. [PubMed: 19559621]
60. Wirthensohn G, Guder WG. Renal substrate metabolism. Physiol Rev. 1986; 66:469–497. [PubMed: 2938198]
61. Bastin J, Cambon N, Thompson M, et al. Change in energy reserves in different segments of the nephron during brief ischemia. Kidney Int. 1987; 31:1239–1247. [PubMed: 3613402]
62. Bagnasco S, Good D, Balaban R, et al. Lactate production in isolated segments of the rat nephron. Am J Physiol. 1985; 248:F522–F526. [PubMed: 3985159]
63. Devalaraja-Narashimha K, Diener AM, Padanilam BJ. Cyclophilin D gene ablation protects mice from ischemic renal injury. Am J Physiol Renal Physiol. 2009; 297:F749–F759. [PubMed: 19553348]
64. Hu W, Chen Z, Ye Z, et al. Knockdown of cyclophilin D gene by RNAi protects rat from ischemia/reperfusion-induced renal injury. Kidney Blood Press Res. 2010; 33:193–199. [PubMed: 20588055]
65. Szeto HH, Liu S, Soong Y, et al. Mitochondria-targeted peptide accelerates ATP recovery and reduces ischemic kidney injury. J Am Soc Nephrol. 2011; 22:1041–1052. [PubMed: 21546574]
66. Molitoris BA, Sutton TA. Endothelial injury and dysfunction: role in the extension phase of acute renal failure. Kidney Int. 2004; 66:496–499. [PubMed: 15253696]
67. Hall AM, Unwin RJ. The not so 'mighty chondrion': emergence of renal diseases due to mitochondrial dysfunction. Nephron Physiol. 2007; 105:1–10.
68. Servais H, Van der SP, Thirion G, et al. Gentamicin-induced apoptosis in LLC-PK1 cells: involvement of lysosomes and mitochondria. Toxicol Appl Pharmacol. 2005; 206:321–333. [PubMed: 16039943]
69. Morales AI, Detaille D, Prieto M, et al. Metformin prevents experimental gentamicin-induced nephropathy by a mitochondria-dependent pathway. Kidney Int. 2010; 77:861–869. [PubMed: 20164825]
70. Shanley PF, Burke TJ. Differential susceptibility to gentamicin toxicity within the proximal convoluted tubule. Ren Fail. 1990; 12:83–87. [PubMed: 2236730]
71. Jobsis PD, Rothstein EC, Balaban RS. Limited utility of acetoxymethyl (AM)-based intracellular delivery systems, *in vivo*: interference by extracellular esterases. J Microsc. 2007; 226:74–81. [PubMed: 17381712]
72. Launay-Vacher V, Izzedine H, Karie S, et al. Renal tubular drug transporters. Nephron Physiol. 2006; 103:97–106.
73. Dunn KW, Sandoval RM, Kelly KJ, et al. Functional studies of the kidney of living animals using multicolor two-photon microscopy. Am J Physiol Cell Physiol. 2002; 283:C905–C916. [PubMed: 12176747]

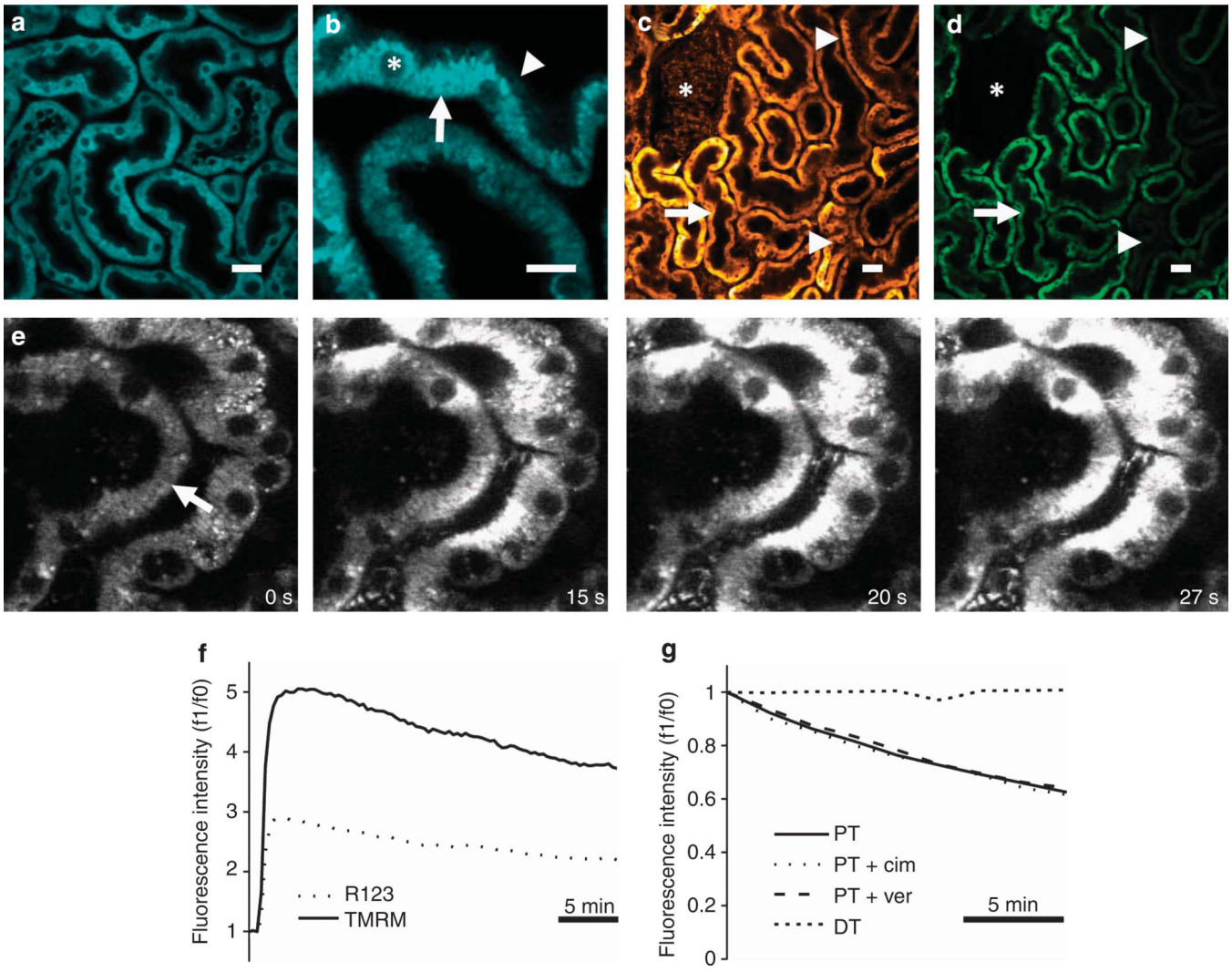

Figure 1. ***In vivo*** **imaging of mitochondrial nicotinamide adenine dinucleotide (NADH) and membrane potential in the kidney**

(**a, b**) Mitochondrial NADH was visible at 720 nm excitation in both mouse (**a**) and rat (**b**) kidneys and showed a characteristic basolateral mitochondrial distribution in tubular cells (arrow), with very little fluorescence signal observed in non-mitochondrial structures including the apical brush border (arrowhead) or cell nuclei (asterisk). (**c–g**) The mitochondrial membrane potential ($\Delta\psi_m$)–dependent dyes tetramethyl rhodamine methyl ester (TMRM) and rhodamine 123 loaded into rodent kidney tubules and localized to the mitochondria; TMRM loaded well into rat proximal tubules (PTs—arrow), distal tubules (DTs—arrowheads), and glomeruli (asterisk) following intravenous injection (**c**), whereas rhodamine 123 loaded well into PTs (arrow), but not DTs (arrowheads) or glomeruli (asterisk) (**d**). Uptake of TMRM into tubules occurred initially from the basolateral side (arrow) (**e**); images depicted were acquired shortly after an intravenous injection of the dye into a mouse. Representative traces are depicted showing the rapid increase and subsequent slow decrease in fluorescence that occurred in rat PTs following intravenous injection of TMRM and rhodamine 123 (**f**). Representative traces are depicted showing that the decline

of TMRM fluorescence in rat PTs was not prevented by prior intravenous injection of either cimetidine or verapamil (**g**); no decline in TMRM fluorescence was observed in DTs. Bars = 20 μm in (**a, b**) and 40 μm in (**c, d**).

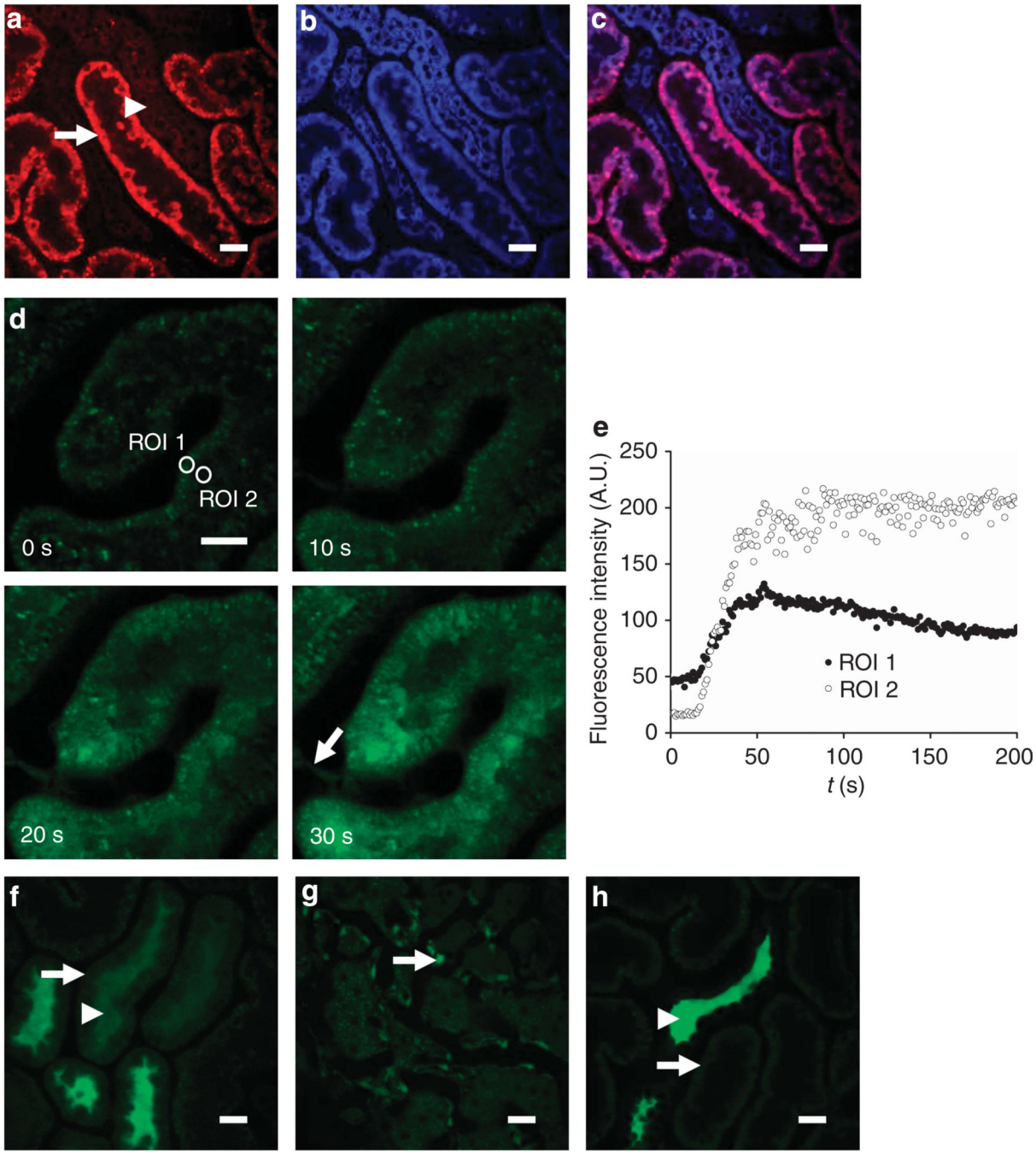

Figure 2. ***In vivo*** **imaging of reactive oxygen species (ROS) production and glutathione in the kidney**

(**a–c**) Imaging of ROS production. Following intravenous injection of the reactive ROS-sensitive dye dihydroethidium (HEt) in rats, the fluorescence signal was higher in proximal tubules (PTs—arrow) than in adjacent distal tubules (DTs—arrowhead) (**a**); simultaneous excitation of mitochondrial nicotinamide adenine dinucleotide (NADH) (blue) (**b**) showed that the two signals colocalized (**c**). (**d–h**) Imaging of intracellular glutathione using monochlorobimane (MCB). Following intravenous injection of MCB in rats, an increase in

fluorescence signal intensity was observed in PTs, which originated at the basolateral aspect of cells and spread apically over time (**d, e**), with simultaneous uptake into endothelial cells (arrow). MCB was subsequently rapidly excreted from PT cells (arrow) into the tubular lumen (arrowhead) (**f**); the image depicted was acquired 8min post injection. Although MCB was excreted by PTs, the signal remained stable in endothelial cells (arrow) (**g**); the image depicted was acquired 18 min post injection. After 20 min, the fluorescence signal had disappeared from PTs (arrow) but was visible in DT lumens (arrowhead) (**h**). Bars = 20 μm in all images.

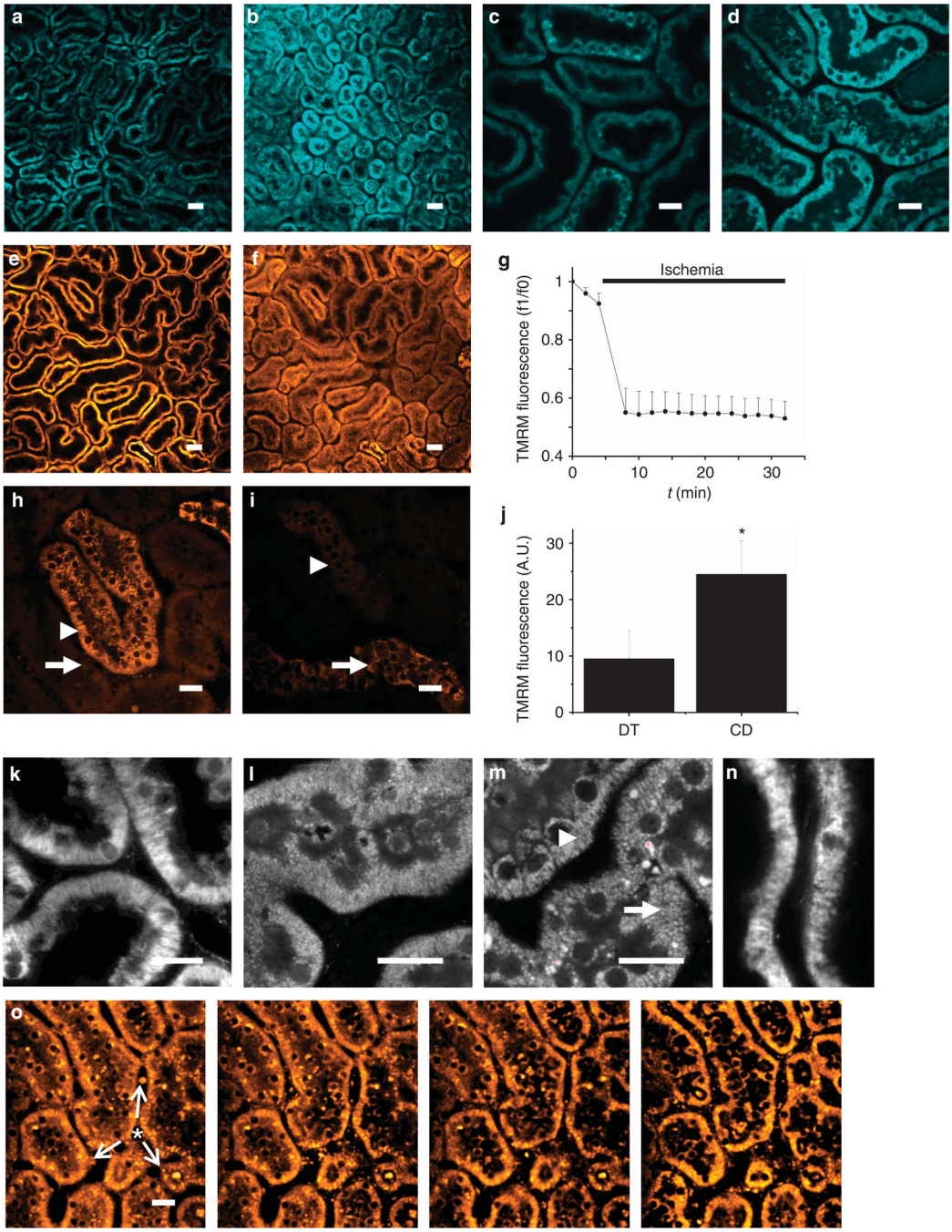

Figure 3. Real-time *in vivo* imaging of mitochondrial structure and function in the kidney during ischemia reperfusion

(**a–d**) Resting nicotinamide adenine dinucleotide (NADH) signal in rat renal cortical tubules (**a**) increased markedly in response to ischemia (**b**); the image depicted was acquired 2min post occlusion of the renal artery; higher resolution images acquired pre- (**c**) and post-ischemia (**d**) confirmed that the signal change was localized to the mitochondria. (**e–g**) In rat proximal tubules (PTs) loaded with tetramethyl rhodamine methyl ester (TMRM), resting mitochondrial membrane potential ($\Delta\psi_m$) (**e**) dissipated rapidly in response to ischemia (**f**);

the image depicted was acquired 2min post ischemia; data depicted in (**g**) are mean (±s.e.m.) mitochondrial TMRM fluorescence intensity in PTs of three separate experiments. $\Delta\psi_m$ was better maintained during ischemia in distal tubules (DTs—arrowhead) than in PTs (arrow) (**h**); the image depicted was acquired 9min post ischemia. After 30 min of ischemia, $\Delta\psi_m$ was better maintained in collecting ducts (arrow) than in DTs (arrowhead) (**i**); data depicted in (**j**) are mean (±s.e.m.) of mitochondrial TMRM fluorescence of three separate experiments (**P*<0.05). (**k–n**) Changes in mitochondrial morphology during ischemia and reperfusion. Images depicted show the following: normal elongated mitochondria in PTs loaded with TMRM (**k**); NADH signal in a PT 10 min post ischemia demonstrating widespread mitochondrial shortening and fragmentation (**l**); NADH signal 30 min post ischemia demonstrating normal mitochondrial morphology in a DT (arrowhead) adjacent to a PT (arrow) (**m**); fragmented mitochondria 20min post reperfusion in a PT loaded with TMRM (**n**). The signal intensity gain was adjusted in images (**k–n**) to optimally visualize mitochondrial structure. (**o**) Repolarization of mitochondria immediately post reperfusion in ischemic PTs preloaded with TMRM; images depicted were acquired 50s apart and demonstrate a spreading wave of repolarization (arrows) from a central blood vessel (asterisk), with reuptake of TMRM from the cytosolic compartment into the mitochondria within cells. Bars = 40 μm in (**a, b**) and (**e, f**) and 20 μm in all other images.

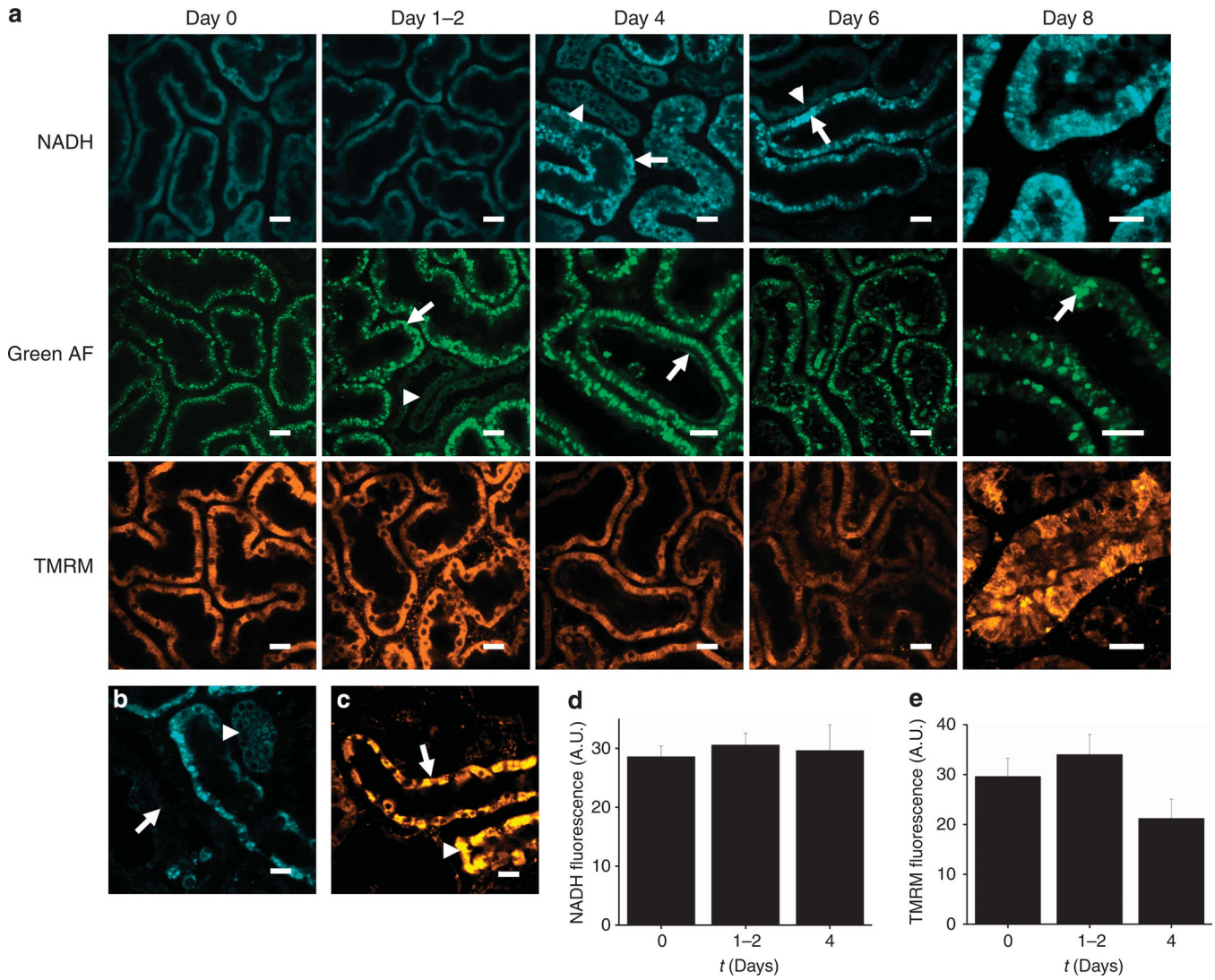

Figure 4. ***In vivo*** **imaging of gentamicin toxicity in the kidney**

(a–c) Representative images are depicted displaying the time course of intracellular changes in gentamicin toxicity. After 1–2 days of exposure, bright structures were visible in the proximal tubules (PTs) in the green autofluorescence (AF) signal (arrow), most likely representing enlarged lysosomes, which were not visible in the distal tubules (DTs—arrowhead); after 4 days, abnormalities were also noted in the PT brush border (arrow). Mitochondrial nicotinamide adenine dinucleotide (NADH) signals remained normal in tubules at 1–2 days; after 4 days, sporadic areas of dysmorphic mitochondria and increased NADH signal were observed in PTs (arrow), but not in DTs (arrowhead). However, the majority of mitochondria in PTs loaded with the mitochondrial membrane potential ($\Delta\psi_m$)–dependent dye tetramethyl rhodamine methyl ester (TMRM) appeared well energized up to 4 days. After 6 days, abnormalities in NADH signal were more widespread in PTs, but remained highly variable, with damaged tubules (arrow) appearing directly adjacent to normal-looking tubules (arrowhead); a high degree of variability was also observed in mitochondrial TMRM signal intensity. After 8 days, mitochondria in the surviving PTs were

grossly dysmorphic, as seen in the NADH image, and massively enlarged lysosomes were visible in the green AF signal (arrow); there were also marked variations in mitochondrial TMRM signal between adjacent cells within surviving PTs. After 8 days of gentamicin exposure, widespread necrosis occurred in PTs, leading to the appearance of ghost tubules devoid of living cells (arrow) (**b**); in contrast, mitochondrial NADH (**b**) and TMRM (**c**) signals remained normal in DTs (arrowhead) and collecting ducts (arrow). (**d, e**) Data depicted show mean mitochondrial NADH (**d**) and TMRM (**e**) fluorescence intensity (±s.e.m.) after exposure to gentamicin; $n = 4$ animals in each group. Bars = 20 mm in all images.